

RESEARCH REPORT

Transcriptomic response of brain tissue to focused ultrasound-mediated blood–brain barrier disruption depends strongly on anesthesia

Alexander S. Mathew¹ | Catherine M. Gorick¹  | E. Andrew Thim¹ |
 William J. Garrison^{1,2} | Alexander L. Klibanov^{1,3} | G. Wilson Miller^{1,2} |
 Natasha D. Sheybani¹ | Richard J. Price^{1,2} 

¹Department of Biomedical Engineering, University of Virginia, Charlottesville, Virginia, USA

²Department of Radiology & Medical Imaging, University of Virginia, Charlottesville, Virginia, USA

³Department of Internal Medicine, Cardiovascular Division, University of Virginia, Charlottesville, Virginia, USA

Correspondence

Richard J. Price and Natasha D. Sheybani,
 Department of Biomedical Engineering, Box
 800759, Health System, University of Virginia,
 Charlottesville, VA 22908.
 Email: rprice@virginia.edu (R. J. P.) nds3sa@
 virginia.edu (N. D. S.)

Funding information

National Cancer Institute, Grant/Award
 Numbers: R01CA197111, F99CA234954;
 National Institute of Biomedical Imaging and
 Bioengineering, Grant/Award Numbers:
 R01EB020147, R21EB024323; National
 Institute of Neurological Disorders and Stroke,
 Grant/Award Number: R01NS111102;
 American Heart Association Fellowship, Grant/
 Award Number: 18PRE34030022; National
 Institutes of Health Training, Grant/Award
 Number: T32LM012416

Abstract

Focused ultrasound (FUS) mediated blood–brain barrier disruption (BBBD) targets the delivery of systemically-administered therapeutics to the central nervous system. Preclinical investigations of BBBD have been performed on different anesthetic backgrounds; however, the influence of the choice of anesthetic on the molecular response to BBBD is unknown, despite its potential to critically affect interpretation of experimental therapeutic outcomes. Here, using bulk RNA sequencing, we comprehensively examined the transcriptomic response of both normal brain tissue and brain tissue exposed to FUS-induced BBBD in mice anesthetized with either isoflurane with medical air (Iso) or ketamine/dexmedetomidine (KD). In normal murine brain tissue, Iso alone elicited minimal differential gene expression (DGE) and repressed pathways associated with neuronal signaling. KD alone, however, led to massive DGE and enrichment of pathways associated with protein synthesis. In brain tissue exposed to BBBD (1 MHz, 0.5 Hz pulse repetition frequency, 0.4 MPa peak-negative pressure), we systematically evaluated the relative effects of anesthesia, microbubbles, and FUS on the transcriptome. Of particular interest, we observed that gene sets associated with sterile inflammatory responses and cell–cell junctional activity were induced by BBBD, regardless of the choice of anesthesia. Meanwhile, gene sets associated with metabolism, platelet activity, tissue repair, and signaling pathways, were differentially affected by BBBD, with a strong dependence on the anesthetic. We conclude that the underlying transcriptomic response to FUS-mediated BBBD may be powerfully

Abbreviations: An, anesthesia; BBB, blood brain barrier; BBBD, blood–brain barrier disruption; CNS, central nervous system; DAMP, damage associated molecular pattern; DGE, differential gene expression; FUS, focused ultrasound; GO, gene ontology; GSEA, gene set enrichment analysis; H&E, hematoxylin and eosin; Iso, isoflurane; Iso-FUS, isoflurane anesthesia with focused ultrasound treatment; KD, ketamine/dexmedetomidine; KD-FUS, ketamine/dexmedetomidine anesthesia with focused ultrasound treatment; LEA, leading edge analysis; MB, microbubbles; MRgFUS, magnetic resonance-guided focused ultrasound; NES, normalized enrichment score; PCA, principal components analysis; PNP, peak-negative pressure; QC, quality control; RBC, red blood cell; RIN, RNA integrity number; SI, sterile inflammation.

This is an open access article under the terms of the Creative Commons Attribution License, which permits use, distribution and reproduction in any medium, provided the original work is properly cited.

© 2020 The Authors. *Bioengineering & Translational Medicine* published by Wiley Periodicals LLC on behalf of American Institute of Chemical Engineers.

influenced by anesthesia. These findings raise considerations for the translation of FUS-BBBD delivery approaches that impact, in particular, metabolism, tissue repair, and intracellular signaling.

KEYWORDS

anesthesia, blood–brain barrier, focused ultrasound, RNA sequencing

1 | INTRODUCTION

The blood–brain barrier (BBB) is essential to maintaining homeostasis in the central nervous system (CNS). The BBB describes a specialized vasculature, consisting of nonfenestrated endothelium, pericytes, astrocytic processes, microglia, and basement membrane working in concert to precisely permit nutrient transport while protecting against toxins and pathogens. However, the BBB also presents a significant neuropharmacological obstacle, preventing 98% of small-molecule therapeutics and nearly 100% of large-molecule therapeutics from accessing the CNS.¹ Significant efforts have focused on strategies to bypass or disrupt the BBB. Methods to bypass the BBB, including intracranial injection and intracerebroventricular infusion, require surgical intervention and thus carry significant risk. Chemical methods to disrupt the BBB, such as mannitol, cause global BBB disruption (BBBD), and lead to considerable neurotoxicity.

Focused ultrasound (FUS) following IV infusion of microbubbles (MB) is a promising approach for BBBD.^{2–4} In this technique, ultrasound waves produced extracorporeally pass through the skull and cause MB circulating in a targeted region of the brain to oscillate. These oscillations disrupt BBB tight junctions and enhance transport of molecules into the brain parenchyma. FUS induced BBBD is an attractive alternative to surgical and chemical methods as it is targeted, noninvasive, and repeatable. Many therapies normally restricted by the BBB have been successfully delivered with FUS + MB, including antibodies,^{5–7} chemotherapeutics,^{8–10} neural stem cells,^{11,12} and genes.^{13–15}

BBBD with FUS is reversible and may be applied in a manner that yields little to no histological damage after repeated treatment.^{3,16,17} However, recent molecular profiling studies have demonstrated that, under certain conditions, FUS induced BBBD can lead to increased expression of pro-inflammatory cytokines, homing receptors, and damage associated molecular patterns (DAMPs) as well as increased systemic macrophage accumulation.¹⁸ These findings are consistent with sterile inflammation (SI), an innate immune response. The potential for FUS to induce local SI has sparked discussion of the cellular implications of FUS, both where additional inflammation may be desirable (such as cancer or Alzheimer's) or undesirable (such as multiple sclerosis or stroke).^{19–22} Transcriptomic studies have shown that FUS induced SI is proportional to both microbubble dose and FUS acoustic pressure.^{23,24} At pressures capable of reliably opening the BBB, as measured by MR contrast enhancement, we previously observed upregulation of proinflammatory transcripts (such as Ccl3, Ccl12, Ccl4, and GFAP) and pathways at 6 h post-FUS, trending toward resolution at 24 h post-FUS, consistent with previous studies.^{18,24,25} Recent

work has demonstrated the extent of post-FUS SI can be modulated by administration of dexamethasone.²⁶ Still, knowledge of the contributions of FUS experimental parameters to the SI response as well as noninflammatory effects on the brain parenchyma remain limited.

One such parameter is general anesthesia. Anesthetic protocols, ubiquitous in preclinical FUS BBBD studies, distinctly impact the circulation time of MB and the extent of FUS-induced vascular damage.^{27,28} Common anesthetics vary widely in their effects on the CNS, differentially affecting cerebral vasculature, neuronal signaling, inflammation, and metabolism.^{29–31} Indeed, a review of the FUS BBBD literature (Table S1) highlights considerable diversity in anesthetic protocols used in preclinical studies of experimental therapeutic efficacy, with isoflurane and ketamine being the most commonly chosen agents. We hypothesize that anesthetics differentially alter the underlying reactivity of the brain parenchyma when FUS is applied, which may produce anesthesia-dependent synergies and conflicts with respect to SI, drug metabolism, or neuronal damage. Herein, we test this hypothesis by detailing the cumulative transcriptome level and pathway level impacts of anesthesia, MB, and FUS on the brain parenchyma.

2 | RESULTS

2.1 | Characterization of FUS-induced BBBD and passive cavitation analysis

Mice were anesthetized with either isoflurane in medical air (Iso) or ketamine/dexmedetomidine (KD) and treated with Magnetic Resonance-guided Focused Ultrasound (MRgFUS) targeted to the right or left striatum ($n = 4$ per group). Contrast-enhanced MRIs (Figure 1(a)), collected before and after treatment, revealed enhanced signal in mice anesthetized with Iso compared to KD (Figure 1(b)). To evaluate MB activity, we analyzed acoustic emissions data obtained from a listening hydrophone embedded in the therapeutic transducer. No significant differences in harmonic emissions (i.e., 2nd, 3rd, and 4th harmonics) or broadband emissions (<10 MHz) were found between Iso and KD (Figure 1(c)).

2.2 | Transcriptomic variation is driven primarily by KD and secondarily by FUS BBBD

Bulk RNA sequencing was performed on mRNA extracted 6 h post-FUS from the treated region of each brain treated with MRgFUS

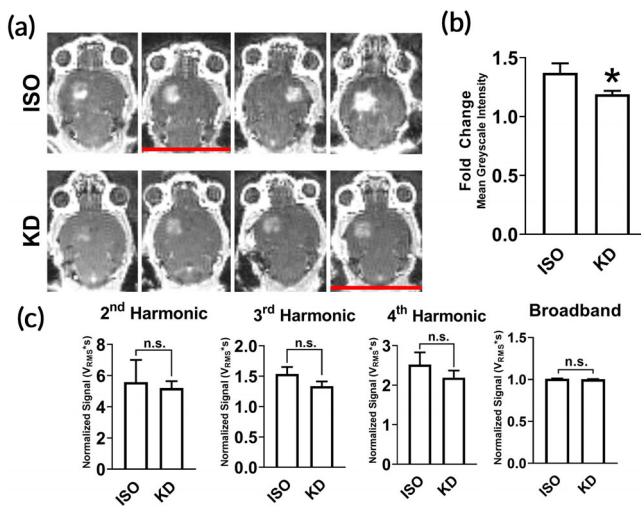


FIGURE 1 Characterization of FUS-induced BBB disruption and passive cavitation analysis. (a) Contrast MR images of naïve brains immediately following BBB disruption with FUS + MB ($n = 4$ per anesthetic). Red lines denote mice that were removed from RNA sequencing analysis due to low RNA integrity number (RIN). (b) Fold difference in mean grayscale signal intensity in contrast-enhanced images in FUS-treated hemisphere relative to contralateral hemisphere. Data are represented as mean with SEM. $*p < 0.05$ ($p = 0.0286$) by Mann-Whitney test. $n = 4$ mice per group. (c) Acoustic emissions signals (2nd, 3rd, and 4th harmonics and broadband) at 0.4 MPa FUS + MB exposure, normalized to 0.005 MPa signal without MB. Data are represented as mean with SEM. No significance was detected by Mann-Whitney test. $n = 4$ mice per group

shown in Figure 1. Brains extracted from naïve mice, mice treated with each anesthetic alone, and mice treated with each anesthetic and MB were also sequenced 6 h after treatment ($n = 3$ per group). After read alignment and QC, principal components analysis (PCA) was performed on transformed transcript counts from each sample to assess global differences between treatment conditions (Figure 2(a)). Interestingly, the first principal component segregated samples by whether they received KD, with Iso-treated mice clustering more closely to the naïve controls. FUS-treated mice formed a distinct cluster only in the KD treated mice. Similar results were obtained when hierarchical clustering was performed on inter-sample Euclidian distances computed between samples based on their transcript counts (Figure 2(b)). With the exception of one sample, the first branch point of the dendrogram separated samples by KD status, while the second and third branch points distinguished samples by FUS treatment.

2.3 | Overview of differential gene expression and gene set enrichment analyses

To evaluate relative transcriptomic differences between conditions, differential gene expression contrasts were computed for all 21 unique combinations of the 7 conditions evaluated (Figure 2(c)). KD alone produced the most profound effect on the transcriptome, with over

3000 genes significantly differentially regulated (p -adjusted < 0.05) compared to naïve brain. Regardless of the anesthetic background, FUS and MB produced moderate (on the order of hundreds of differentially expressed genes) and negligible (< 9 differentially expressed genes) effects on gene expression, respectively. Iso alone had a marginal effect on the transcriptome, only significantly changing the expression of 26 genes. Next, we performed gene set enrichment analysis (GSEA) to identify biological processes consistent with genes differentially expressed within each contrast (Figure 2(d)). GSEA was performed using the Gene Ontology (GO) Biological Pathways database, wherein each “GO” term represents a collection of genes associated with a particular biological phenomenon. Surprisingly, Iso alone affected more biological pathways than KD, despite KD affecting considerably more genes. The addition of MB changed relatively few biological pathways. FUS had the strongest effect on biological pathways on both anesthetic backgrounds, inducing more pathways than it repressed.

2.4 | Anesthetics differentially affect the transcriptome of normal brain tissue

The relative transcriptional impact of Iso and KD on the mouse striatum was marked, with Iso significantly changing expression of 26 genes compared to the 3291 significantly changed by KD (Figure 3(a)). Iso alone induced a traditional anesthetic transcriptional program of repression of neuronal activity (Figure 3(b)). KD, however, had a minimal effect on these pathways, instead enriching for steps of protein synthesis and targeting (Figure 3(c)). These trends persisted upon addition of MB or FUS. To assess the effect of anesthesia on neuroinflammation, we examined GO processes related to inflammation differentially changed by Iso or KD alone (Figure 3(d)). Both anesthetics enriched the CCR Chemokine Receptor Binding pathway, while only Iso induced the Leukocyte Migration pathway. The addition of FUS + MB led to further activation of both inflammatory pathways. Iso alone also had a unique effect on development pathways, downregulating neuronal development (likely due to repressing neuronal signaling) and upregulating development of glial cells, oligodendrocytes, and vasculature (Figure 3(e)). In general, addition of MB or MB + FUS led to loss of significance of these pathways. To identify which transcripts contributed to the enrichment or repression of particular pathways, we performed leading edge analysis (LEA). *Pecam1* (CD31) was identified as the most significant gene driving the enrichment of the CCR Chemokine Receptor Binding, Leukocyte Migration, and Vasculature Development pathways. Indeed, *Pecam1* is one of the few genes induced by Iso with an adjusted p -value less than 0.05.

2.5 | Anesthetics differentially affect the transcriptome of brain tissue exposed to FUS BBB

We next sought to compare gene expression changes induced by FUS BBB when performed under Iso (Iso-FUS) versus KD (KD-FUS). First,

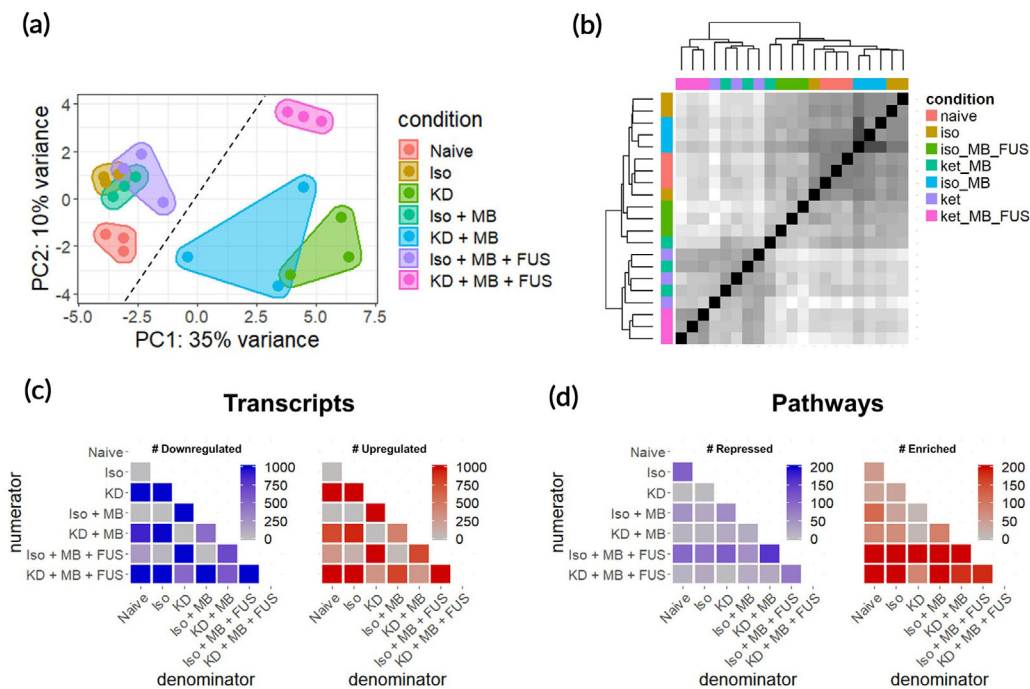


FIGURE 2 RNA sequencing overview. (a) Principal components analysis of RNA-seq transcript counts after variance stabilizing transformation. Each dot represents a single sample ($n = 3$ per group). The dashed line separates KD- samples (left of line) from KD+ samples (right of line). (b) Pairwise sample Euclidean distance matrix computed on transcript counts. Each row and column represents a single sample. Hierarchical clustering was performed using complete linkage. Darker shade corresponds to increasing transcriptome similarity. (c) Number of significantly downregulated (left) and upregulated genes (right) for all 21 contrasts of the 7 conditions tested. Each row represents a numerator condition and each column represents a denominator condition. (d) Magnitude of significantly repressed (left) and enriched pathways (right) for all 21 contrasts of the 7 conditions tested. Each row represents a numerator condition and each column represents a denominator condition. For all genes and pathways, significance is defined as p -adjusted <0.05

we evaluated the extent and overlap of differentially expressed genes (Figure 4(a)) and differentially regulated pathways (Figure 4(b)), controlling for changes due to anesthesia + MB alone. While more genes were differentially regulated by KD-FUS, more gene sets were significantly enriched/repressed by Iso-FUS. Interestingly, despite minimal intersection of transcript identities between the two BBBB conditions, 41% of the pathways significantly induced by KD-FUS were also significantly induced by Iso-FUS. Second, we identified 6 categories of biological pathways consistently changed by Iso-FUS, KD-FUS, or both (Figure 4(c)). Regardless of the anesthetic background, FUS led to enrichment of genes involved in endothelial cell activity, including pathways associated with cell-cell adhesion and angiogenesis. Iso-FUS induced these pathways more significantly, and additionally led to the expression of genes associated with leukocyte adhesion. Similarly, both FUS conditions led to activation of many inflammation pathways, with the breadth and depth of these responses substantially enhanced in the Iso-FUS condition. Notably, the MHC class I and MHC class II antigen processing and presentation pathways were only upregulated when comparing KD-FUS treated mice to naïve controls. We found the most significant divergence between Iso-FUS and KD-FUS when comparing metabolic pathways. Iso-FUS led to repression of broad and specific metabolic programs while several of these were enriched by KD-FUS. Consistent with significant inflammation and endothelial activation, platelet activity was enhanced by Iso-FUS,

while these pathways were relatively unchanged by KD-FUS. Gene sets associated with tissue repair were enriched by FUS under both anesthetics and those associated with neurogenesis were additionally upregulated by KD-FUS only. Signaling pathways engaged by FUS treatment independent of anesthesia included VEGFR signaling, Wnt signaling, and the NF- κ B signaling pathway. STAT, SAPK, dopamine, and integrin signaling were further enriched only in Iso-FUS contrasts.

To further compare the effect of anesthesia on FUS BBBB, we performed LEA on selected gene sets enriched by both Iso-FUS and KD-FUS. Comparing transcripts in the LEA of the (Iso + MB + FUS)/(Iso + MB) contrast against those in LEA of the (KD + MB + FUS)/(KD + MB) contrast for the same pathway allows us to address whether FUS is achieving the same “end” (pathway enrichment) by similar “means” (transcript regulation) on different anesthetic backgrounds. We performed comparative LEA on gene sets associated with cell-cell junctions and inflammation, as these were the most consistently induced by both Iso-FUS and KD-FUS. Out of the 173 genes in the Cell Junction Organization gene set (GO:0034330), Iso-FUS and KD-FUS enriched 48 and 50, respectively (Figure 4(d)). 19 transcripts were found in the leading edge of both anesthetics including *Cdh5* (VE-Cadherin), *Vcl*, and *Flt1*. While all 3 of these transcripts were significantly upregulated by KD-FUS across multiple contrasts, only *Cdh5* was significantly upregulated by FUS under Iso. Notably, when compared to naïve controls alone, KD alone significantly downregulated *Flt1* and KD + MB led to a trending decrease (p -adj = 0.06).

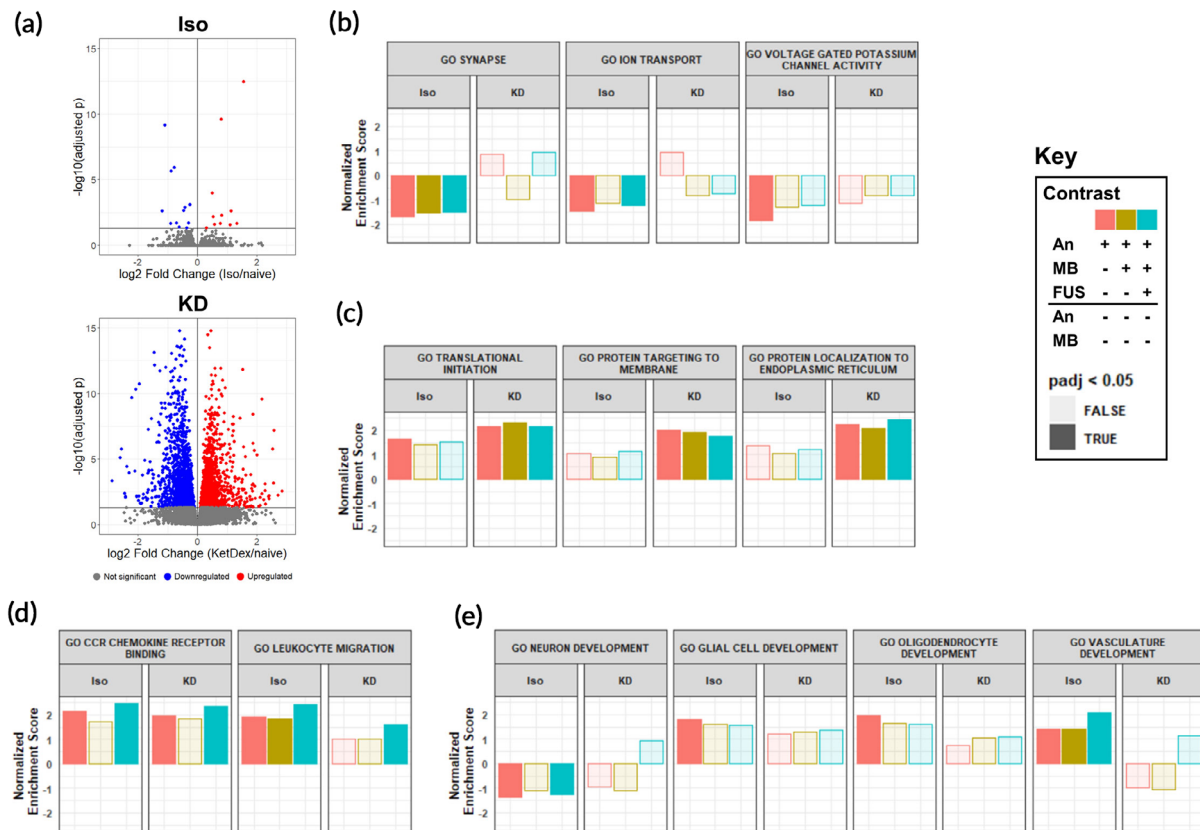


FIGURE 3 Anesthetics differentially affect the transcriptome of normal brain tissue. (a) Volcano plots of differentially regulated transcripts 6 h post anesthesia delivery with Iso (top) or KD (bottom) compared to naïve controls. (b–e) Normalized Enrichment scores (NES) for gene sets associated with (b) neuronal signaling, (c) protein synthesis, (d) inflammation, and (e) development. GSEA was computed based on ranked DGE from (An, red), An + MB (blue), and An + MB + FUS (gold) against naïve controls for Iso and KD. Opaque bars indicate an adjusted p -value <0.05

We next compared the LEA overlap on the Immune System Process gene set (GO:0002682), a broad collection of 1709 genes associated with the immune system (Figure 4(e)). Iso-FUS and KD-FUS enriched 512 and 304 of these, respectively, with 103 genes enriched by both. IL-1 α was found in both LEAs and significantly upregulated across multiple contrasts while IL-1 β was only found in the Iso-FUS LEA and indeed only significantly upregulated in Iso-only FUS contrasts. TNF α was found in both LEAs to be significantly upregulated by FUS under both anesthetics when compared to naïve controls, and trending upward in other FUS contrasts (Log2FC >2, unadjusted p -value <0.1 for Iso + MB + FUS vs Iso, Iso + MB + FUS vs Iso + MB, KD + MB + FUS vs. KD, and KD + MB + FUS vs. KD + MB contrasts). To narrow the scope of immune system-related LEA overlaps, we repeated this analysis on the Chemokine Activity gene set (GO:0008009) which only contains 34 genes (Figure 4(f)). Iso-FUS and KD-FUS enriched 16 and 12 chemokines, respectively, 7 of which were shared. Iso-FUS induced the strongest Ccl2 upregulation regardless of the control condition. KD alone induced a comparable upregulation of Ccl2 with no additional effect due to FUS. Cxcl16 however was more strongly induced with KD-FUS than Iso-FUS when controlling for anesthetic. Ccl3 was upregulated by FUS under both anesthetics as well as KD alone. In summary, while FUS promotes phenotypes such as cell junction organization, inflammation, and

chemokine activity independent of anesthetic, the nature of the transcripts mediating these effects are often anesthesia-dependent.

2.6 | Anesthetics differentially affect transcripts associated with BBB structure and function

We next evaluated the effects of anesthesia, MB, and FUS on transcripts known to be associated with the BBB.³² Iso-FUS upregulated transcripts mediating leukocyte adhesion, including E-selectin, P-selectin, and Icam1 (Figure 5(a)). Icam1 was also upregulated by KD alone when compared to sham and by KD-FUS when compared to KD or KD + MB. With respect to BBB tight junction transcripts, FUS upregulated Cldn5 and Emp1 independent of anesthetic (Figure 5(b)). KD alone led to downregulation of Ocln and Tjp1. We next evaluated the effect of our experimental conditions on BBB transporter transcripts and observed heterogeneous effects (Figure 5(c)). In general, KD led to significantly more DGE in this category than Iso, with very few transcripts changing their expression due to FUS or MB on either anesthetic background. This trend was even more extreme when evaluating BBB transcripts involved in transcytosis and other miscellaneous functions (Figure 5(d)); KD was the only variable significantly changing the expression of transcripts in this class.

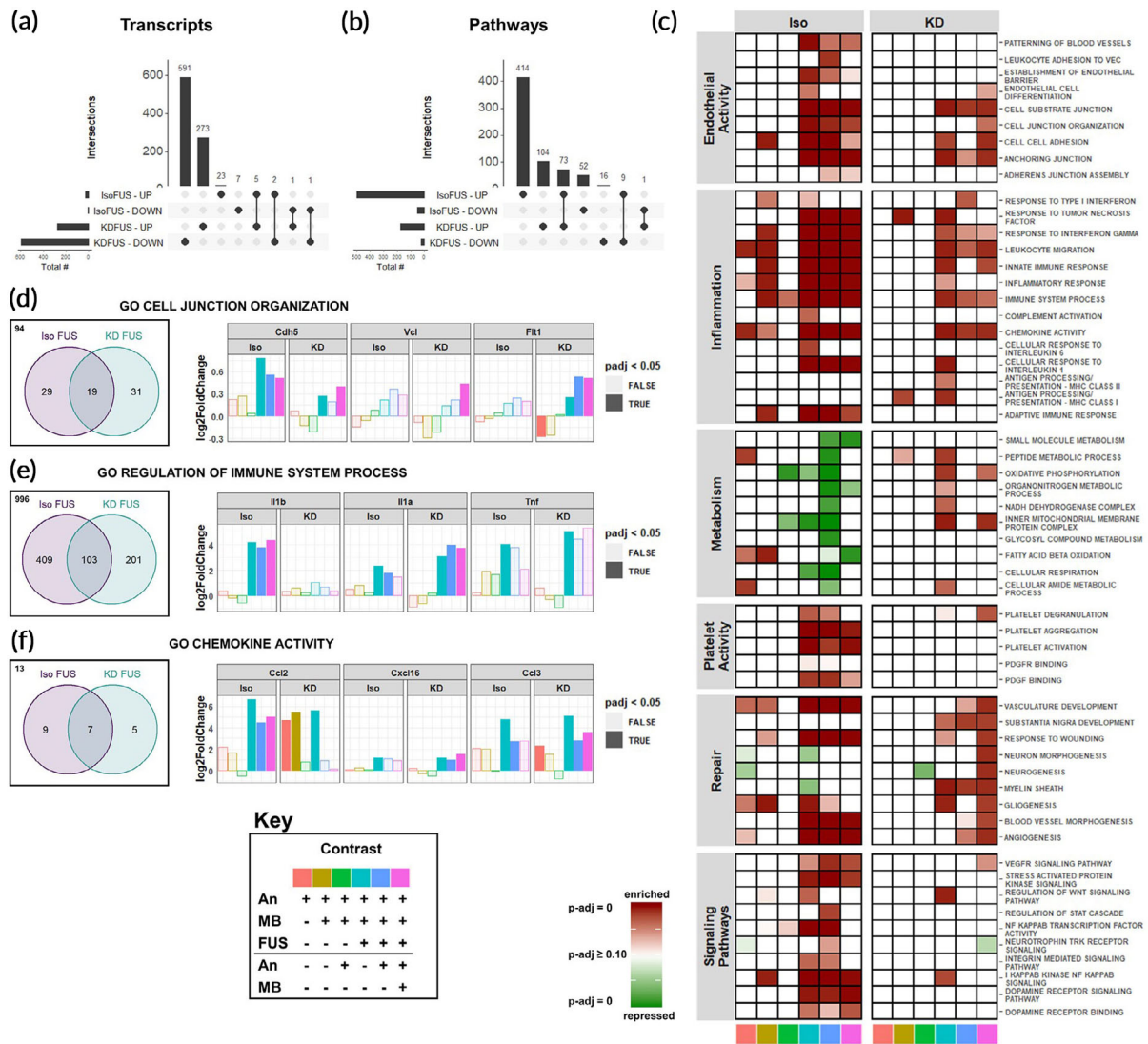


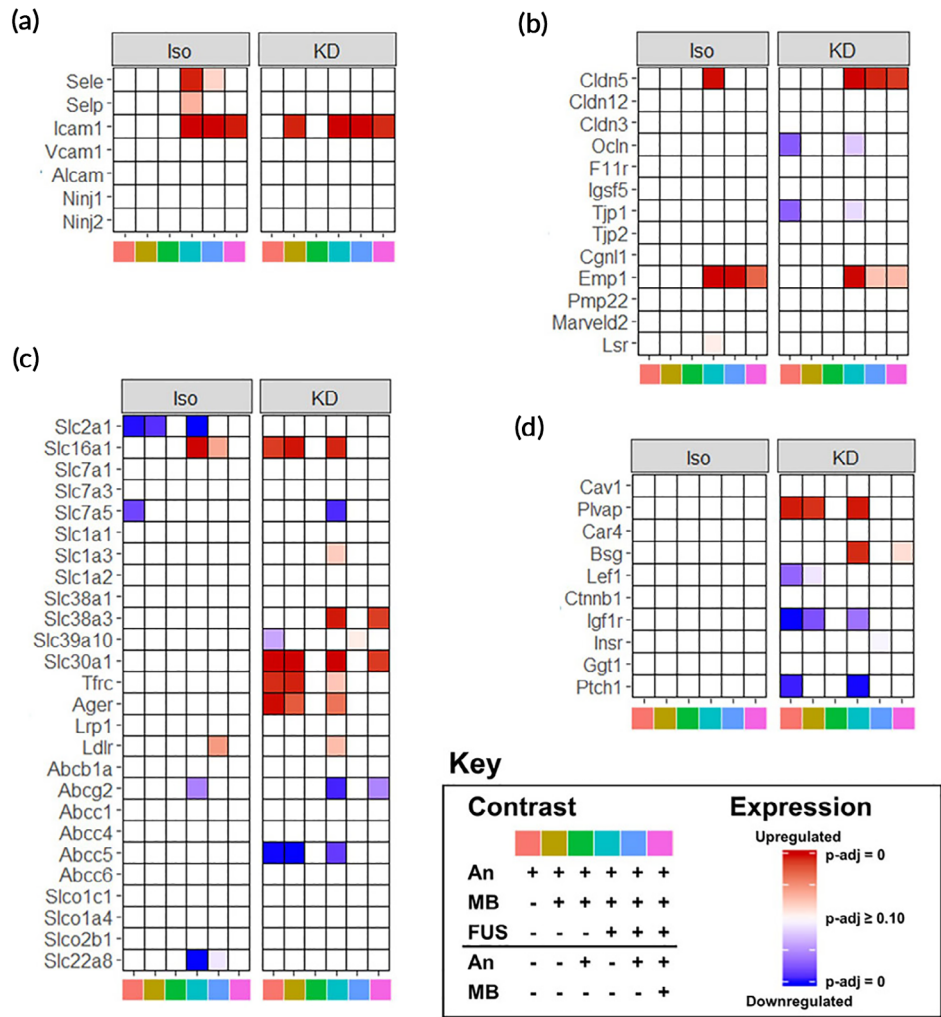
FIGURE 4 Anesthetics differentially affect the transcriptomic response of brain tissue exposed to FUS BBBD. (a) UpSetR plots for evaluating intersections of upregulated and downregulated transcripts between IsoFUS and KDFUS, controlling for the effects of anesthesia and MB. (b) UpSetR plots for evaluating intersections of enriched and repressed pathways between IsoFUS and KDFUS, controlling for the effects of anesthesia and MB alone. (c) Heatmap showing significance of repression (green) or enrichment (red) of pathways (rows) associated with endothelial activity, inflammation, metabolism, platelet activity, repair, and signaling for multiple contrasts (columns), separated by anesthetic. Contrast identities are shown by the color at the bottom of the column, corresponding to the key. Full opacity corresponds to an adjusted-*p*-value of 0, while full transparency corresponds to an adjusted *p*-value ≥ 0.10 . (d–f) Venn diagrams (left) of leading edge transcripts and selected leading edge transcript expression (right) for (d) Cell Junction Organization (GO:0034330), (e) Regulation of Immune Process (GO:0002682), and (f) Chemokine Activity (GO:0008009) gene sets, separated by anesthetic background. Bar color represents the contrast, corresponding to the key. Opaque bars indicate an adjusted *p*-value < 0.05 . Each color in the key corresponds to a specific pairwise comparison of Anesthesia (An), An + MB, and An + MB + FUS for either Iso or KD, specifying the numerator (above the black line), and denominator (below the black line). For example, pink corresponds to the ratio of gene expression for mice treated with An + MB + FUS to those treated with just An + MB

2.7 | Tissue damage elicited by FUS BBBD is minimal and not affected by anesthetic

Given the anesthesia-dependence of BBBD and FUS-induced gene expression, we next tested whether anesthesia affected the extent of damage in the brain parenchyma after treatment with the same FUS pressure. We performed histological analysis of murine brains treated with combinations of Iso, KD, and FUS (Figures 6(a–d)).

Brains treated at 0.8 MPa (twice the acoustic pressure of our standard BBBD protocol) were used as positive controls for damage. We scored multiple transverse sections from each condition for RBC extravasation and vacuolation (Figure 6(e)). With the exception of the 0.8 MPa positive control group, all conditions tested elicited minimal damage. Thus, BBBD using these conditions elicits little to no histological damage, independent of whether Iso or KD is used.

FIGURE 5 Anesthetics differentially affect transcripts associated with BBB structure and function. (a–d) Heatmaps of significance of upregulation (red) or downregulation (blue) for selected genes (rows) across multiple contrasts (columns), separated by anesthetic for transcripts associated with BBB structure and function. Selected categories include (a) leukocyte adhesion, (b) BBB tight junctions, (c) transporters, and (d) transcytosis/miscellaneous. Contrast identities are shown by the color at the bottom of the column, corresponding to the key. Full opacity corresponds to an adjusted-*p*-value of 0, while full transparency corresponds to an adjusted *p*-value ≥ 0.10 . Each color in the key corresponds to a specific pairwise comparison of Anesthesia (An), An + MB, and An + MB + FUS for either Iso or KD, specifying the numerator (above the black line), and denominator (below the black line). For example, pink corresponds to the ratio of gene expression for mice treated with An + MB + FUS to those treated with just An + MB



3 | DISCUSSION

BBBD mediated by FUS-activated MB has emerged as a promising technique for the image-guided and noninvasive delivery of therapeutics to the CNS. Though this procedure is safe, our understanding of cellular responses to FUS BBBD at the transcriptional level is still limited. This knowledge gap becomes especially significant when considering that preclinical BBBD studies have been performed on a multitude of different anesthetic backgrounds (Table S1), a factor that could affect the interpretation of how experimental therapeutic outcomes will translate to human applications, wherein such anesthetics are not utilized. Our study systematically addressed how choice of general anesthetic shapes acute transcriptomic responses to FUS with respect to SI, endothelial activity, metabolism, platelet activity, repair, molecular signaling, and BBB-associated genes (see summary in Table 1). Ultimately, we conclude that the underlying transcriptomic response to FUS-mediated BBBD may be strongly influenced by the choice of anesthetic. Such responses may synergize and/or conflict with responses generated by the therapeutic approach itself. Thus, our results provide a framework for rational anesthesia selection for preclinical BBBD studies and will likely find utility when comparing

clinical outcomes to preclinical results for FUS mediated BBBD drug and gene delivery approaches.

PCA and hierarchical clustering performed on variance-stabilizing transformed RNA-seq counts data revealed the relative contributions of Iso, KD, MB, and FUS to intersample variability with respect to CNS gene expression (Figure 2(a),(b)). The most striking of these was KD, inducing DGE (*p*-adjusted < 0.05) of 3291 genes when compared to naïve controls (Figure 3(a)). Whether this profound change in gene expression is attributable to ketamine, dexmedetomidine, or both is unclear. Microarray studies of developing rat brain have shown a similar magnitude of acute differential gene expression from ketamine alone.³³ More specifically, investigators reported 819 differentially expressed genes with fold change > 1.4 , *p*-adj < 0.05 compared to the 1182 meeting these criteria in our study at an identical timepoint. Though ketamine's mechanism of action is still unclear, recent studies into its rapid anti-depressant action suggest ketamine indirectly suppresses eukaryotic elongation factor 2 kinase (eEf2K), leading to increased protein translation.³⁴ This mechanism is in agreement with our pathway level findings (Figure 3(c)). Though fewer transcriptomic level studies exist for dexmedetomidine, it is known to acutely augment transcriptional programs associated with inflammation and

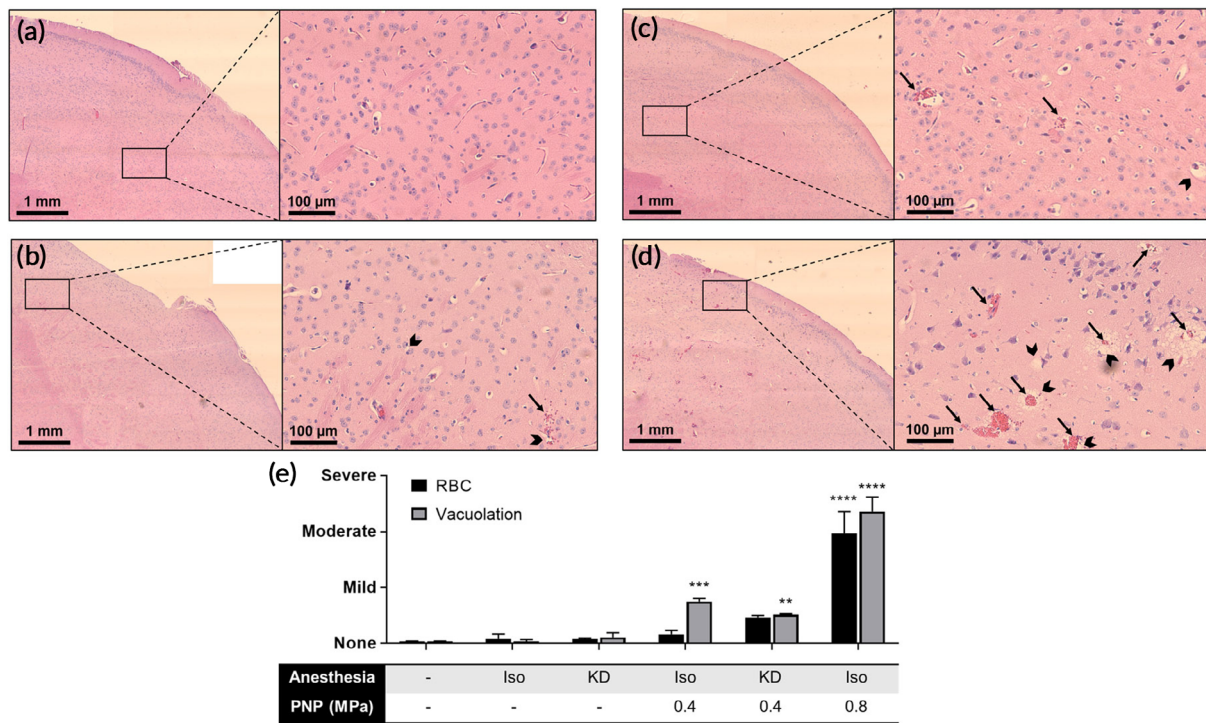


FIGURE 6 Tissue damage elicited by FUS BBBB is minimal and not affected by anesthetic. Representative 4× stitched (left) and 20× (right) H&E images of murine right striatum either (a) untreated or treated with (b) IsoMA-FUS at 0.4 MPa, (c) KD-FUS at 0.4 MPa, or (d) IsoMA-FUS at 0.8 MPa. Arrows indicate RBC extravasation, chevrons indicate vacuolation. (e) Scoring of RBC extravasation (black bars) and vacuolation (grey bars). Data are represented as mean ± SEM. ** $p < 0.01$, *** $p < 0.001$, **** $p < 0.00001$ by one-way ANOVA followed by comparison against naïve with Dunnett's multiple comparison test. $n = 2-3$ per group

TABLE 1 Summary of transcriptional responses

Response	ISO/naïve	KD/naïve	(ISO + MB + FUS)/(ISO + MB)	(KD + MB + FUS)/(KD + MB)
Transcriptional impact	—	↑↑↑	↑↑	↑↑
Endothelial activity	—	—	↑↑↑	↑↑↑
Inflammation	↑	—	↑↑↑	↑↑
Metabolism	↑↑	—	↓↓	↑
Platelet activity	—	—	↑↑↑	↑
Repair	↑	—	↑↑	↑↑↑
Signaling pathways	↓	—	↑↑↑	—

circadian rhythm.^{35,36} In stark contrast to KD, we found Iso had a negligible impact on gene expression, only significantly altering the expression of 26 genes. This finding is in close agreement with existing acute transcriptomic studies of inhalable anesthetics in rats, which report between 0 and 20 differentially expressed genes.^{37,38} Interestingly, despite weak changes in expression magnitude, Iso changed regulation of significantly more pathways than KD (Figure 2(d)). We thus hypothesize that, while Iso influences more targeted transcriptional programs, the combination of ketamine and dexmedetomidine elicits wide-ranging, complex transcription thereby preventing GSEA from detecting discrete pathway enrichment.

We observed increases in inflammatory signatures elicited by both anesthetics (Figure 3(d)). Of the few genes upregulated by Iso

alone, a surprising number were immune-associated. Some examples include upregulation of T-cell associated markers Ly6a and Ctl2a, upregulation of adhesion markers Pecam1 and CD93, and downregulation of Nfkb, the protein product of which inhibits NF- κ B. Indeed, activation of NF- κ B has been proposed as a mechanism by which volatile anesthetics elicit neuroinflammation^{39,40}. Several rodent studies have demonstrated volatile anesthetics can also acutely induce expression of IL-6, IL-1 β , and activated caspase-3.⁴¹⁻⁴⁴ Under conditions of CNS stress, including ischemia or LPS exposure, volatile anesthetics attenuate inflammation, suggesting that these drugs may contribute to maintaining homeostasis in the brain, rather than being strictly pro- or anti-inflammatory.⁴⁵⁻⁴⁸ KD also induced signatures associated with inflammation, though to a lesser extent

and with a less clear mechanism than Iso. At the chemokine level, for example, KD significantly upregulated Ccl17, Ccl2, Ccl3, and Ccl6 with minor but significant downregulation of Cxcl12 and Cx3cl1. These mixed effects may be caused by contrasting neuroinflammatory effects produced by ketamine and dexmedetomidine. Ketamine has been shown to be acutely inflammatory in naïve mice, increasing levels of IL-6, IL-1 β , and TNF- α ,⁴⁹ while Dexmedetomidine tends to protect against neuroinflammation.⁵⁰⁻⁵³ The ability of each anesthetic to amplify or protect against SI induced by FUS may be an important experimental consideration for future preclinical FUS work.

SI caused by FUS-activated MB has raised concerns over its feasibility for repeated clinical application. SI can last for at least 24 h after a single sonication, and is dependent on MB dose and FUS pressure.^{18,23-25} Proposed causes of SI include direct acoustic force damage, ischemia reperfusion injury due to vasospasm, and leakage of blood into the parenchyma.^{18,23-25} Our unbiased analyses suggest a confluence of these mechanisms that can be affected by choice of anesthetic (Figure 4(c)). Pathways enriched by both Iso-FUS and KD-FUS clearly indicate extensive cytokine production, possibly initiated by DAMP release and pattern recognition receptor (PRR) signaling. In general, Iso-FUS led to more extensive activation of the immune response compared to KD-FUS, enriching signatures associated with NF- κ B signaling, consistent with previous studies.^{18,23,25} However even for pathways with similar enrichment, LEA suggests anesthesia affects the quality of FUS-induced SI. The anesthesia dependent induction of IL-1 β and IL-1 α provides an example (Figure 4(e)). Though they bind to the same receptor, they have fundamentally different upstream triggers and downstream consequences. IL-1 α is constitutively expressed. It possesses both intracellular activity as a proinflammatory transcription factor and extracellular activity as a DAMP.^{54,55} IL-1 β , however, is induced by NOD-, LRR-, and pyrin domain-containing protein 3 (NLRP3) inflammasome activation.⁵⁶ Importantly, these two cytokines recruit different populations of myeloid cells and represent distinct stages of the SI response.⁵⁷ Thus, anesthesia may impact the temporal relationship between FUS application and SI. Enrichment of junctional assembly pathways, VEGF signaling, and angiogenesis supports FUS-induced activation of endothelial cells, leading to both recruitment of leukocytes and barrier repair, especially under Iso. Of note, we observed significant upregulation of claudin-5 transcript, whose tight junction protein product is essential to BBB integrity, in both FUS groups. This may indicate initiation of transcriptional programs to repair the disrupted barrier (Figure 5(b)). In contrast, a microarray study of brain microvessels did not detect significant differences in claudin-5 post-FUS.²⁵ This discrepancy could be due to differences in species (i.e., mouse vs. rat), the source of the analyzed tissue in the brain, anesthesia protocol, and several FUS and microbubble parameters. Downregulation of multiple metabolic pathways in Iso-FUS contrasts further suggests Iso may prime the BBB for more significant alteration than KD.

Despite differential responses at the transcriptional level and in MRI signal enhancement (Figure 1), FUS applied under both anesthetics led to little to no generation of petechiae by H&E (Figure 6). With respect to coagulation signatures by RNA-seq, only Iso-FUS led

to increased platelet activity despite no significant difference in RBC extravasation compared to KD-FUS (Figure 4(c)). While Iso has minimal effect on platelet activity,⁵⁸⁻⁶⁰ both ketamine and dexmedetomidine reduce coagulability.⁶¹⁻⁶⁴ Thus, KD may minimize the inflammatory response resulting from blood products in the brain parenchyma compared to Iso upon FUS application.

Transient SI can provide beneficial effects in certain disease contexts with respect to clearance and regeneration.⁶⁵ Indeed, this may be the primary mechanism by which FUS promotes A β plaque clearance in Alzheimer's disease.⁶⁶ Similarly, neurogenesis observed after FUS may be attributable to tissue repair mechanisms preceded SI.^{67,68} We observed activation of repair mechanisms by FUS, though to different extents depending on the anesthetic chosen. The observation that KD promotes stronger signatures of repair and weaker signatures of inflammation, endothelial activation, coagulation, and metabolic alteration supports its use over Iso for pathologies where further CNS stress is undesirable.

Our investigation has some limitations. First, RNA-sequencing only provides transcript-level information. mRNA may not always correlate proportionally to protein expression.⁶⁹⁻⁷² This risk is mitigated at the pathway level, where we present significant alteration of large families of genes consistently up or downregulated by FUS and/or anesthesia. Further, the high intragroup consistency along with the absolute magnitude of differential gene or pathway level changes make noise an unlikely driver of the diverse changes we observed. However, because RNA-seq was performed on bulk tissue, it is not easy to distinguish changes in transcription from changes in relative cell numbers. Next, whether transcriptional changes in Iso-FUS mice are a consequence of isoflurane's interaction with FUS or enhanced BBB permeability is unclear. Finally, not all experiments were performed on the same FUS-system. Though transducer frequencies and acoustic pressures were matched between systems, it is possible that differences in transducer geometries produced confounders in experimental endpoints.

4 | CONCLUSIONS

We investigated how Iso and KD, the two most commonly used anesthetics in preclinical FUS BBB studies, differentially affect CNS responses to FUS-activated MB. At the same acoustic pressure, FUS induced similar profiles of MB cavitation and measures of damage regardless of the anesthetic. RNA sequencing performed acutely after treatment with combinations of Iso, KD, MB, and FUS revealed distinct contributions from each. Specifically, while Iso alone produced transcriptomic profiles nearly identical to those of naïve mice, it also elicited stronger signatures of stress in the neurovascular unit when combined with FUS. KD, however, induced sweeping transcriptome changes alone, but blunted markers of SI while promoting gene sets associated with tissue repair upon FUS application compared to Iso-FUS. These results provide important context for previous preclinical FUS studies, and underscore anesthesia as an important experimental variable to consider for future work.

5 | MATERIALS AND METHODS

5.1 | Animals

11 week old female C57BL/6 mice were purchased from Jackson and maintained on a 12/12 h light/dark cycle. Mice weighed between 22 and 28 g and were given food and water *ad libitum*. All animal experiments were approved by the Animal Care and Use Committee at the University of Virginia and conformed to the National Institutes of Health regulations for the use of animals in research.

5.2 | Anesthesia

Mice in groups designated “KD” received 50–70 mg/kg Ketamine and 0.25–0.5 mg/kg Dexmedetomidine via intraperitoneal injection with no additional maintenance or reversal drug given. Mice in groups designated as “Iso” or “Iso-MA” were placed in an induction chamber and received isoflurane delivered to effect in concentrations of 2.5% in medical air using a vaporizer. For isoflurane groups, anesthesia was maintained via nosecone for a total of 90 min.

5.3 | MRgFUS mediated BBBD

An MRgFUS system was used to treat brains for RNA-seq studies. Once mice were anesthetized, a tail vein catheter was inserted to permit intravenous injections of MBs and the MRI contrast agent. The heads of the mice were shaved and depilated, and the animals were then placed in a supine position over a degassed water bath coupled to an MR-compatible small animal FUS system (RK-100; FUS Instruments, Toronto, Canada). The entire system was then placed in a 3T MR scanner (Magnetom Prisma; Siemens Medical Solutions, Malvern, Pennsylvania). A 3.5 cm diameter receive RF coil, designed and built in-house, was placed around the head to maximize imaging SNR. Baseline three-dimensional T1-weighted MR images were acquired at 0.3 mm resolution using a short-TR spoiled gradient-echo pulse sequence and used to select 4 FUS target locations in and around the right or left striatum.

Mice received an injection of albumin-shelled MBs (1×10^5 MBs/g b.w.), formulated as previously described.^{14,73,74} Briefly, MBs consist of an albumin protein shell and an octofluoropropane gas core. While made in-house, these MBs are similar to Optison™ ultrasound contrast agent. A Beckman Coulter counter was used to determine the MB concentration and size distribution. The mean diameter of the bubbles was 2.32 μm (SD = 1.41 μm), with 90% of the bubbles <4.09 μm . The stock concentration was 2.6E9 MBs/ml, but the bubbles were diluted to a concentration of 1E5 MBs/g b.w. in 50 μl of saline just prior to injection. MBs were delivered via a single bolus injection. Sonication began immediately after clearance of the catheter. Sonications (4 spots in a 2 \times 2 grid) were performed at 0.4 MPa peak-negative pressure (PNP) using a 1.1 MHz single element focused transducer (FUS Instruments, Toronto, Canada) operating in 10 ms

bursts, 0.5 Hz pulse repetition frequency and 2 min total duration. A voltage-pressure calibration is provided in Figure S2. Immediately following the FUS treatment, mice received an intravenous injection of gadolinium-based contrast agent (0.05 ml of 105.8 mg/ml preparation; Multihance; Bracco Diagnostics), and contrast-enhanced images were acquired to assess BBBD using the same T1-weighted pulse sequence mentioned above.

5.4 | Passive cavitation detection

Acoustic emissions were detected with a 2.5 mm wideband unfocused hydrophone mounted in the center of the transducer. Acoustic signal was captured using a scope card (ATS460, Alazar, Pointe-Claire, Canada) and processed using an in-house MATLAB (MathWorks) algorithm. Acoustic emissions at the fundamental frequency, harmonics (2f, 3f, 4f), sub harmonic (0.5f), and ultra-harmonics (1.5f, 2.5f, 3.5f) were assessed by first taking the root mean square of the peak spectral amplitude (V_{rms}) in each frequency band after applying a 200 Hz bandwidth filter, and then summing the product of V_{rms} and individual sonication duration over the entire treatment period. Broadband emissions were assessed by summing the product of V_{rms} and individual sonication duration for all remaining emissions over the entire treatment period.

5.5 | Bulk RNA sequencing and analysis

Six hours after treatment, mice were euthanized via an overdose of pentobarbital sodium and phenytoin sodium. Immediately following euthanasia, the mouse brains were harvested and the anterior right quadrants (~100 mg) were excised (with the exception of 1 mouse, which had FUS treatment on the left). For FUS-treated mice, contrast MR images were referenced to confirm extraction of the full volume of sonicated brain. A representative 3D image of the harvested tissue is provided in Figure S1. Harvested tissue was placed in RNAlater (Qiagen), and stored at -80°C . RNA extraction was performed using the RNeasy Mini Kit (Qiagen). mRNA was isolated using the NEBNext Poly(A) mRNA Magnetic Isolation Module (New England Biolabs, Ipswich, Massachusetts) followed by library preparation using the NEBNext Ultra II Directional RNA Library Prep Kit for Illumina (New England Biolabs). Sequencing was performed using a NextSeq 500 (Illumina, San Diego, California) at a target depth of 25 million 2×75 bp paired end reads per sample. Reads were quasi-mapped to the mouse genome (mm10 assembly) and quantified at the transcript level using Salmon v0.11.2⁷⁵ followed by summary to the gene level using tximport v1.10.1.⁷⁶ Differential gene expression was performed with DESeq2 v1.22.2.⁷⁷ Gene set enrichment analysis was performed with the GO Biological Processes^{78,79} gene sets fromMSigDB³² using FGSEA v1.8.0⁸⁰ run with 100,000 permutations. 4-group intersections were visualized with UpSetR plots.⁸¹ All other plots were generated in Figures 2–5 were generated using ggplot2 unless otherwise specified.⁸²

5.6 | Stereotactic FUS mediated BBBB

A stereotactic tabletop FUS system was used to treat brains for histological studies. Sonications using the stereotactic frame were performed using a 1-MHz spherical-face single-element FUS transducer with a diameter of 4.5 cm (Olympus). FUS (0.4 or 0.8 MPa; 120 s, 10-ms bursts, 0.5-Hz burst rate) was targeted to the right striatum. The 6-dB acoustic beamwidths along the axial and transverse directions are 15 and 4 mm, respectively. The waveform pulsing was driven by a waveform generator (AFG310; Tektronix) and amplified using a 55-dB RF power amplifier (ENI 3100LA; Electronic Navigation Industries). A voltage-PNP calibration is provided in Figure S2.

Once anesthetized, a tail-vein catheter was inserted to permit i.v. injections of MBs and Evans Blue. The heads of the mice were shaved and depilated, and the animals were then positioned prone in a stereotactic frame (Stoelting). The mouse heads were ultrasonically coupled to the FUS transducer with ultrasound gel and degassed water and positioned such that the ultrasound focus was localized to the right striatum. Mice received an i.v. injection of the MBs (1×10^5 MBs/g b.w.) and Evans Blue, followed by 0.1 ml of 2% heparinized saline to clear the catheter. Sonication began immediately after clearance of the catheter. In contrast to the MR-guided experiments, which targeted four spots, only one location was targeted in these studies due to the increased focal region of the transducer (4 mm in the transverse direction, relative to 1 mm for the transducer in the MR-compatible system).

5.7 | Histological processing and analysis

Sixty minutes after Evans Blue injection, mice were euthanized via an overdose of pentobarbital sodium and phenytoin sodium. A macroscopic image was taken immediately after whole brain harvest. Brains were then placed in 10% NBF, embedded in paraffin, and sectioned 400 μ m apart. H&E stained sections were imaged with 4 \times and 20 \times objectives on an Axioskop light microscope (Zeiss, Germany) equipped with a PROGRES GRYPAX microscope camera (Jenoptik, Germany). Ten 20 \times images from the region of the right striatum with maximal Evans Blue extravasation were taken per section and 2–6 sections were imaged per brain. A researcher blinded to treatment condition assigned a semi-quantitative score of 0 (none—complete absence of RBC extravasation/vacuolation), 1 (mild—sparse small sites of RBC extravasation/vacuolation), 2 (moderate—singular large OR multiple small sites of RBC extravasation/vacuolation), or 3 (severe—multiple large sites of RBC extravasation/vacuolation) to each 20 \times image for RBC extravasation and vacuolation using a custom MATLAB (MathWorks) script.

5.8 | Statistical methods

For contrast enhancement and acoustic emissions analyses, data are presented as mean \pm SEM. Statistical significance was assessed by

Mann–Whitney test. For differential gene expression significance analysis, DESeq2⁷⁵ was used with default parameters. Briefly, DESeq2 pools expression information across all replicates and fits a negative binomial model to each gene followed by a Wald test. An independent filtering process combined with automatic outlier detection using Cook's distance maximize the number of significant genes remaining after FDR correction. Only genes with FDR adjusted p -values <0.05 are presented as significant unless stated otherwise. For GSEA, the fgsea⁸⁰ tool was implemented with 100,000 permutations. Briefly, statistical significance for each pathway is evaluated with a permutation test followed by standard FDR correction. Only enrichment scores with FDR adjusted p -values <0.05 are presented as significant unless stated otherwise. For histological analyses, data are presented as mean \pm SEM. Statistical significance was detected by one-way ANOVA followed by comparison against naïve with Dunnett's multiple comparison test.

ACKNOWLEDGMENTS

Supported by National Institutes of Health Grants R01EB020147, R01CA197111, R01NS111102, and R21EB024323 to Richard J. Price and R01EB023055 to Alexander L. Klivanov. Alexander S. Mathew was supported by National Institutes of Health Training Grant T32LM012416. Catherine M. Gorick was supported by American Heart Association Fellowship 18PRE34030022 and a UVA School of Medicine Wagner Fellowship. Natasha D. Sheybani was supported by a National Cancer Institute F99/K00 Predoctoral to Postdoctoral Fellow Transition Award (F99CA234954), NSF Graduate Research Fellowship, and a UVA School of Medicine Wagner Fellowship. The authors thank the UVA Genome and Technology Core for their assistance with sample processing.

CONFLICT OF INTEREST

The authors declare no conflict of interest.

AUTHOR CONTRIBUTIONS

Conceptualization: Alexander S. Mathew, Catherine M. Gorick, Natasha D. Sheybani, E. A. Thim, and Richard J. Price; *Methodology:* Alexander S. Mathew, Catherine M. Gorick, Natasha D. Sheybani, E. A. Thim, William J. Garrison, Alexander L. Klivanov, G. W. Miller, and Richard J. Price; *Investigation:* Alexander S. Mathew, Catherine M. Gorick, Natasha D. Sheybani, E. A. Thim, William J. Garrison, Alexander L. Klivanov, G. W. Miller, and Richard J. Price; *Formal Analysis:* Alexander S. Mathew, Catherine M. Gorick, Natasha D. Sheybani, E. A. Thim, and Richard J. Price; *Writing—Original Draft Preparation:* Alexander S. Mathew and Richard J. Price; *Writing—Review & Editing:* Alexander S. Mathew, Catherine M. Gorick, Natasha D. Sheybani, E. A. Thim, William J. Garrison, Alexander L. Klivanov, G. W. Miller, and Richard J. Price; *Supervision; Funding Acquisition:* Alexander S. Mathew and Richard J. Price

ORCID

Catherine M. Gorick  <https://orcid.org/0000-0002-0139-3438>

Richard J. Price  <https://orcid.org/0000-0002-0237-2102>

REFERENCES

- Pardridge WM. The blood-brain barrier: bottleneck in brain drug development. *NeuroRx*. 2005;2(1):3-14. <https://doi.org/10.1602/neuroRx.2.1.3>.
- Choi JJ, Pernot M, Small SA, Konofagou EE. Noninvasive, transcranial and localized opening of the blood-brain barrier using focused ultrasound in mice. *Ultrasound Med Biol*. 2007;33(1):95-104. <https://doi.org/10.1016/j.ultrasmedbio.2006.07.018>.
- Hynynen K, McDannold N, Sheikov NA, Jolesz FA, Vykhodtseva N. Local and reversible blood-brain barrier disruption by noninvasive focused ultrasound at frequencies suitable for trans-skull sonications. *Neuroimage*. 2005;24(1):12-20. <https://doi.org/10.1016/j.neuroimage.2004.06.046>.
- Hynynen K, McDannold N, Vykhodtseva N, Jolesz FA. Noninvasive MR imaging-guided focal opening of the blood-brain barrier in rabbits. *Radiology*. 2001;220(3):640-646. <https://doi.org/10.1148/radiol.2202001804>.
- Kinoshita M, McDannold N, Jolesz FA, Hynynen K. Noninvasive localized delivery of herceptin to the mouse brain by MRI-guided focused ultrasound-induced blood-brain barrier disruption. *Proc Natl Acad Sci U S A*. 2006;103(31):11719-11723. <https://doi.org/10.1073/pnas.0604318103>.
- Park EJ, Zhang YZ, Vykhodtseva N, McDannold N. Ultrasound-mediated blood-brain/blood-tumor barrier disruption improves outcomes with trastuzumab in a breast cancer brain metastasis model. *J Control Release*. 2012;163(3):277-284. <https://doi.org/10.1016/j.jconrel.2012.09.007>.
- Janowicz PW, Leinenga G, Götz J, Nisbet RM. Ultrasound-mediated blood-brain barrier opening enhances delivery of therapeutically relevant formats of a tau-specific antibody. *Sci Rep*. 2019;9(1):1-9. <https://doi.org/10.1038/s41598-019-45577-2>.
- McDannold N, Zhang Y, Supko JG, et al. Acoustic feedback enables safe and reliable carboplatin delivery across the blood-brain barrier with a clinical focused ultrasound system and improves survival in a rat glioma model. *Theranostics*. 2019;9(21):6284-6299. <https://doi.org/10.7150/thno.35892>.
- Aryal M, Vykhodtseva N, Zhang Y-Z, Park J, McDannold N. Multiple treatments with liposomal doxorubicin and ultrasound-induced disruption of blood-tumor and blood-brain barriers improve outcomes in a rat glioma model. *J Control Release*. 2013;169(1-2):103-111. <https://doi.org/10.1016/j.jconrel.2013.04.007>.
- Liu HL, Hua MY, Chen PY, et al. Blood-brain barrier disruption with focused ultrasound enhances delivery of chemotherapeutic drugs for glioblastoma treatment. *Radiology*. 2010;255(2):415-425. <https://doi.org/10.1148/radiol.10090699>.
- Shen W-B, Anastasiadis P, Nguyen B, et al. Magnetic enhancement of stem cell-targeted delivery into the brain following mr-guided focused ultrasound for opening the blood-brain barrier. *Cell Transplant*. 2017;26(7):1235-1246. <https://doi.org/10.1177/0963689717715824>.
- Burgess A, Ayala-Grosso CA, Ganguly M, et al. Targeted delivery of neural stem cells to the brain using MRI-guided focused ultrasound to disrupt the blood-brain barrier. Ikezu T, ed. *PLoS One*. 2011;6(11):e27877. <https://doi.org/10.1371/journal.pone.0027877>.
- Stavarache MA, Petersen N, Jurgens EM, et al. Safe and stable noninvasive focal gene delivery to the mammalian brain following focused ultrasound. *J Neurosurg*. 2018;130(3):1-10. <https://doi.org/10.3171/2017.8.JNS17790>.
- Mead BP, Kim N, Miller GW, et al. Novel Focused ultrasound gene therapy approach noninvasively restores dopaminergic neuron function in a rat Parkinson's Disease Model. *Nano Lett*. 2017;17(6):3533-3542. <https://doi.org/10.1021/acs.nanolett.7b00616>.
- Lin CYCJ, Lin CYCJ, Lin YT, et al. Microbubble-facilitated ultrasound pulsation promotes direct α -synuclein gene delivery. *Biochem Biophys Res Commun*. 2019;517(1):77-83. <https://doi.org/10.1016/j.bbrc.2019.07.017>.
- Choi JJ, Selert K, Gao Z, Samiotaki G, Baseri B, Konofagou EE. Noninvasive and localized blood-brain barrier disruption using focused ultrasound can be achieved at short pulse lengths and low pulse repetition frequencies. *J Cereb Blood Flow Metab*. 2011;31(2):725-737. <https://doi.org/10.1038/jcbfm.2010.155>.
- McDannold N, Vykhodtseva N, Raymond S, Jolesz FA, Hynynen K. MRI-guided targeted blood-brain barrier disruption with focused ultrasound: histological findings in rabbits. *Ultrasound Med Biol*. 2005;31(11):1527-1537. <https://doi.org/10.1016/j.ultrasmedbio.2005.07.010>.
- Kovacs ZI, Kim S, Jikaria N, et al. Disrupting the blood-brain barrier by focused ultrasound induces sterile inflammation. *Proc Natl Acad Sci*. 2017;114(1):E75-E84. <https://doi.org/10.1073/PNAS.1614777114>.
- Silburt J, Lipsman N, Aubert I. Disrupting the blood-brain barrier with focused ultrasound: perspectives on inflammation and regeneration. *Proc Natl Acad Sci U S A*. 2017;114(33):E6735-E6736. <https://doi.org/10.1073/pnas.1710761114>.
- Kovacs ZI, Burks SR, Frank JA. Reply to Silburt et al.: concerning sterile inflammation following focused ultrasound and microbubbles in the brain. *Proc Natl Acad Sci U S A*. 2017;114(33):E6737-E6738. <https://doi.org/10.1073/pnas.1711544114>.
- McMahon D, Hynynen K. Reply to Kovacs et al.: concerning acute inflammatory response following focused ultrasound and microbubbles in the brain. *Theranostics*. 2018;8(8):2249-2250. <https://doi.org/10.7150/thno.25468>.
- Kovacs ZI, Burks SR, Frank JA. Focused ultrasound with microbubbles induces sterile inflammatory response proportional to the blood brain barrier opening: attention to experimental conditions. *Theranostics*. 2018;8(8):2245-2248. <https://doi.org/10.7150/thno.24181>.
- McMahon D, Hynynen K. Acute inflammatory response following increased blood-brain barrier permeability induced by focused ultrasound is dependent on microbubble dose. *Theranostics*. 2017;7(16):3989-4000. <https://doi.org/10.7150/thno.21630>.
- Gorick CM, Mathew AS, Garrison WJ, et al. Sonoselective transfection of cerebral vasculature without blood-brain barrier disruption. *Proc Natl Acad Sci*. 2020;117(11):5644-5654. <https://doi.org/10.1073/PNAS.1914595117>.
- McMahon D, Bendayan R, Hynynen K. Acute effects of focused ultrasound-induced increases in blood-brain barrier permeability on rat microvascular transcriptome. *Sci Rep*. 2017;7(1):45657. <https://doi.org/10.1038/srep45657>.
- McMahon D, Oakden W, Hynynen K. Investigating the effects of dexamethasone on blood-brain barrier permeability and inflammatory response following focused ultrasound and microbubble exposure. *Theranostics*. 2020;10(4):1604-1618. <https://doi.org/10.7150/thno.40908>.
- McDannold N, Zhang Y, Vykhodtseva N. Blood-brain barrier disruption and vascular damage induced by ultrasound bursts combined with microbubbles can be influenced by choice of anesthesia protocol. *Ultrasound Med Biol*. 2011;37(8):1259-1270. <https://doi.org/10.1016/j.ultrasmedbio.2011.04.019>.
- Mullin L, Gessner R, Kwan J, Kaya M, Borden MA, Dayton PA. Effect of anesthesia carrier gas on in vivo circulation times of ultrasound microbubble contrast agents in rats. *Contrast Media Mol Imaging*. 2011;6(3):126-131. <https://doi.org/10.1002/cmimi.414>.
- Velayudha Reddy S. Effect of general anesthetics on the developing brain. *J Anaesthesiol Clin Pharmacol*. 2012;28(1):6-10. <https://doi.org/10.4103/0970-9185.92426>.
- Istaphanous GK, Loepke AW. General anesthetics and the developing brain. *Curr Opin Anaesthesiol*. 2009;22(3):368-373. <https://doi.org/10.1097/ACO.0b013e3283294c9e>.

31. Loepke AW, Soriano SG. An assessment of the effects of general anesthetics on developing brain structure and neurocognitive function. *Anesth Analg*. 2008;106(6):1681-1707. <https://doi.org/10.1213/ane.0b013e318167ad77>.
32. Liberzon A, Subramanian A, Pinchback R, Thorvaldsdóttir H, Tamayo P, Mesirov JP. Molecular signatures database (MSigDB) 3.0. *Bioinformatics*. 2011;27(12):1739-1740. <https://doi.org/10.1093/bioinformatics/btr260>.
33. Liu FG, Paule M, Ali S, Wang C. Ketamine-induced neurotoxicity and changes in gene expression in the developing rat brain. *Curr Neuropharmacol*. 2011;9(1):256-261. <https://doi.org/10.2174/157015911795017155>.
34. Monteggia LM, Gideons E, Kavalali ET. The role of eukaryotic elongation factor 2 kinase in rapid antidepressant action of ketamine. *Biol Psychiatry*. 2013;73(12):1199-1203. <https://doi.org/10.1016/j.biopsych.2012.09.006>.
35. Wittner M, Sivenius J, Koistinaho J. α 2-Adrenoreceptor agonist, dexmedetomidine, alters acute gene expression after global ischemia in gerbils. *Neurosci Lett*. 1997;232(2):75-78. [https://doi.org/10.1016/S0304-3940\(97\)00585-5](https://doi.org/10.1016/S0304-3940(97)00585-5).
36. Yoshida Y, Nakazato K, Takemori K, Kobayashi K, Sakamoto A. The influences of propofol and dexmedetomidine on circadian gene expression in rat brain. *Brain Res Bull*. 2009;79(6):441-444. <https://doi.org/10.1016/j.brainresbull.2009.04.015>.
37. Sakamoto A, Imai JI, Nishikawa A, et al. Influence of inhalation anesthesia assessed by comprehensive gene expression profiling. *Gene*. 2005;356(1-2):39-48. <https://doi.org/10.1016/j.gene.2005.03.022>.
38. Pan JZ, Wei H, Hecker JG, Tobias JW, Eckenhoff RG, Eckenhoff MF. Rat brain DNA transcript profile of halothane and isoflurane exposure. *Pharmacogenet Genomics*. 2006;16(3):171-182. <https://doi.org/10.1097/01.fpc.0000189795.21770.08>.
39. Li Z, Ni C, Xia C, et al. Calcineurin/nuclear factor- κ B signaling mediates isoflurane-induced hippocampal neuroinflammation and subsequent cognitive impairment in aged rats. *Mol Med Rep*. 2017;15(1):201-209. <https://doi.org/10.3892/mmr.2016.5967>.
40. Zhang L, Zhang J, Yang L, Dong Y, Zhang Y, Xie Z. Isoflurane and sevoflurane increase interleukin-6 levels through the nuclear factor-kappa B pathway in neuroglioma cells. *BJA Br J Anaesth*. 2013;110 (suppl_1):i82-i91. <https://doi.org/10.1093/bja/aet115>.
41. Wu X, Lu Y, Dong Y, et al. The inhalation anesthetic isoflurane increases levels of proinflammatory TNF- α , IL-6, and IL-1 β . *Neurobiol Aging*. 2012;33(7):1364-1378. <https://doi.org/10.1016/j.neurobiolaging.2010.11.002>.
42. Xie Z, Culley DJ, Dong Y, et al. The common inhalation anesthetic isoflurane induces caspase activation and increases amyloid β -protein level in vivo. *Ann Neurol*. 2008;64(6):618-627. <https://doi.org/10.1002/ana.21548>.
43. Cao L, Li L, Lin D, Zuo Z. Isoflurane induces learning impairment that is mediated by interleukin 1 β in rodents. *PLoS One*. 2012;7(12):e51431. <https://doi.org/10.1371/journal.pone.0051431>.
44. Lin D, Cao L, Wang Z, Li J, Washington JM, Zuo Z. Lidocaine attenuates cognitive impairment after isoflurane anesthesia in old rats. *Behav Brain Res*. 2012;228(2):319-327. <https://doi.org/10.1016/j.bbr.2011.12.010>.
45. Plachinta RV, Hayes JK, Cerilli LA, Rich GF. Isoflurane pretreatment inhibits lipopolysaccharide-induced inflammation in rats. *Anesthesiology*. 2003;98(1):89-95. <https://doi.org/10.1097/0000542-20030100-00017>.
46. Chung IS, Kim JA, Kim JA, et al. Reactive Oxygen species by isoflurane mediates inhibition of nuclear factor κ B activation in lipopolysaccharide-induced acute inflammation of the lung. *Anesth Analg*. 2013;116(2):327-335. <https://doi.org/10.1213/ANE.0b013e31827aec06>.
47. Li H, Yin J, Li L, Deng J, Feng C, Zuo Z. Isoflurane postconditioning reduces ischemia-induced nuclear factor- κ B activation and interleukin 1 β production to provide neuroprotection in rats and mice. *Neurobiol Dis*. 2013;54:216-224. <https://doi.org/10.1016/j.nbd.2012.12.014>.
48. Blum FE, Zuo Z. Volatile anesthetics-induced neuroinflammatory and anti-inflammatory responses. *Med Gas Res*. 2013;3(1):16. <https://doi.org/10.1186/2045-9912-3-16>.
49. Li Y, Shen R, Wen G, et al. Effects of ketamine on levels of inflammatory cytokines IL-6, IL-1 β , and TNF- α in the hippocampus of mice following acute or chronic administration. *Front Pharmacol*. 2017;8 (MAR):139. <https://doi.org/10.3389/fphar.2017.00139>.
50. Yeh C-H, Hsieh L-P, Lin M-C, Wei T-S, Lin H-C, Chang C-C, Hsing C-H. Dexmedetomidine reduces lipopolysaccharide induced neuroinflammation, sickness behavior, and anhedonia. *PLOS ONE*. 2018; 13(1):e0191070. <https://doi.org/10.1371/journal.pone.0191070>.
51. Huang C, Ng OTW, Chu JMT, et al. Differential effects of propofol and dexmedetomidine on neuroinflammation induced by systemic endotoxin lipopolysaccharides in adult mice. *Neurosci Lett*. 2019;707: 134309. <https://doi.org/10.1016/j.neulet.2019.134309>.
52. Peng M, Wang YL, Wang CY, Chen C. Dexmedetomidine attenuates lipopolysaccharide-induced proinflammatory response in primary microglia. *J Surg Res*. 2013;179(1):e219-e225. <https://doi.org/10.1016/j.jss.2012.05.047>.
53. Zhu YJ, Peng K, Meng XW, Ji FH. Attenuation of neuroinflammation by dexmedetomidine is associated with activation of a cholinergic anti-inflammatory pathway in a rat tibial fracture model. *Brain Res*. 2016;1644:1-8. <https://doi.org/10.1016/j.brainres.2016.04.074>.
54. Cohen I, Rider P, Carmi Y, et al. Differential release of chromatin-bound IL-1 α discriminates between necrotic and apoptotic cell death by the ability to induce sterile inflammation. *Proc Natl Acad Sci U S A*. 2010;107(6):2574-2579. <https://doi.org/10.1073/pnas.0915018107>.
55. Werman A, Werman-Venkert R, White R, et al. The precursor form of IL-1 α is an intracrine proinflammatory activator of transcription. *Proc Natl Acad Sci U S A*. 2004;101(8):2434-2439. <https://doi.org/10.1073/pnas.0308705101>.
56. Dinarello CA. Overview of the IL-1 family in innate inflammation and acquired immunity. *Immunol Rev*. 2018;281(1):8-27. <https://doi.org/10.1111/imr.12621>.
57. Rider P, Carmi Y, Guttman O, et al. IL-1 α and IL-1 β recruit different myeloid cells and promote different stages of sterile inflammation. *J Immunol*. 2011;187(9):4835-4843. <https://doi.org/10.4049/jimmunol.1102048>.
58. Dogan IV, Ovali E, Eti Z, Yayci A, Gogus FY. The in vitro effects of isoflurane, sevoflurane, and propofol on platelet aggregation. *Anesth Analg*. 1999;88(2):432-436. <https://doi.org/10.1213/0000539-199902000-00039>.
59. Hirakata H, Nakamura K, Sai S, et al. Platelet aggregation is impaired during anaesthesia with sevoflurane but not with isoflurane. *Can J Anaesth*. 1997;44(11):1157-1161. <https://doi.org/10.1007/BF03013337>.
60. Law NL, Ng KFJ, Irwin MG, Man JSF. Comparison of coagulation and blood loss during anaesthesia with inhaled isoflurane or intravenous propofol. *BJA Br J Anaesth*. 2001;86(1):94-98. <https://doi.org/10.1093/bja/86.1.94>.
61. Atkinson PM, Taylor DI, Chetty N. Inhibition of platelet aggregation by ketamine hydrochloride. *Thromb Res*. 1985;40(2):227-234. [https://doi.org/10.1016/0049-3848\(85\)90333-0](https://doi.org/10.1016/0049-3848(85)90333-0).
62. Undar A, Eichstaedt HC, Clubb FJ Jr, et al. Anesthetic induction with ketamine inhibits platelet activation before, during, and after cardiopulmonary bypass in baboons. *Artif Organs*. 2004;28(10):959-962. <https://doi.org/10.1111/j.1525-1594.2004.07377.x>.
63. Nakagawa T, Hirakata H, Sato M, et al. Ketamine suppresses platelet aggregation possibly by suppressed inositol triphosphate formation and subsequent suppression of cytosolic calcium increase. *Anesthesiology*. 2002;96:1147-1152.

64. Chen Z, Shao DH, Mao ZM, Shi LL, Ma XD, Zhang DP. Effect of dexmedetomidine on blood coagulation in patients undergoing radical gastrectomy under general anesthesia. *Med (United States)*. 2018;97(27):e11444. <https://doi.org/10.1097/MD.00000000000011444>.
65. Kim YK, Na KS, Myint AM, Leonard BE. The role of pro-inflammatory cytokines in neuroinflammation, neurogenesis and the neuroendocrine system in major depression. *Prog Neuro-Psychopharmacology Biol Psychiatry*. 2016;64:277-284. <https://doi.org/10.1016/j.pnpbp.2015.06.008>.
66. Leinenga G, Götz J. Scanning ultrasound removes amyloid- β and restores memory in an Alzheimer's disease mouse model. *Sci Transl Med*. 2015;7(278):278ra33. <https://doi.org/10.1126/scitranslmed.aaa2512>.
67. Scarcelli T, Jordano JF, O'Reilly MA, Ellens N, Hynynen K, Aubert I. Stimulation of hippocampal neurogenesis by transcranial focused ultrasound and microbubbles in adult mice. *Brain Stimul*. 2014;7(2):304-307. <https://doi.org/10.1016/j.brs.2013.12.012>.
68. Mooney SJ, Shah K, Yeung S, Burgess A, Aubert I, Hynynen K. Focused ultrasound-induced neurogenesis requires an increase in blood-brain barrier permeability. *PLoS One*. 2016;11(7):e0159892. <https://doi.org/10.1371/journal.pone.0159892>.
69. Nie L, Wu G, Zhang W. Correlation between mRNA and protein abundance in *Desulfovibrio vulgaris*: a multiple regression to identify sources of variations. *Biochem Biophys Res Commun*. 2006;339(2):603-610. <https://doi.org/10.1016/j.bbrc.2005.11.055>.
70. Gygi SP, Rochon Y, Franza BR, Aebersold R. Correlation between protein and mRNA abundance in yeast. *Mol Cell Biol*. 1999;19(3):1720-1730. <https://doi.org/10.1128/mcb.19.3.1720>.
71. Chen G, Gharib TG, Huang CC, et al. Discordant protein and mRNA expression in lung adenocarcinomas. *Mol Cell Proteomics*. 2002;1(4):304-313. <https://doi.org/10.1074/mcp.M200008-MCP200>.
72. Maier T, Güell M, Serrano L. Correlation of mRNA and protein in complex biological samples. *FEBS Lett*. 2009;583(24):3966-3973. <https://doi.org/10.1016/j.febslet.2009.10.036>.
73. Nance E, Timbie K, Miller GW, et al. Non-invasive delivery of stealth, brain-penetrating nanoparticles across the blood-brain barrier using MRI-guided focused ultrasound. *J Control Release*. 2014;189(0):123-132. <https://doi.org/10.1016/j.jconrel.2014.06.031>.
74. Mead BP, Mastorakos P, Suk JS, Klivanov AL, Hanes J, Price RJ. Targeted gene transfer to the brain via the delivery of brain-penetrating DNA nanoparticles with focused ultrasound. *J Control Release*. 2016;223:109-117. <https://doi.org/10.1016/j.jconrel.2015.12.034>.
75. Patro R, Duggal G, Love MI, Irizarry RA, Kingsford C. Salmon provides fast and bias-aware quantification of transcript expression. *Nat Methods*. 2017;14(4):417-419. <https://doi.org/10.1038/nmeth.4197>.
76. Sonesson C, Love MI, Robinson MD. Differential analyses for RNA-seq: transcript-level estimates improve gene-level inferences. *F1000Research*. 2016;4:1521. <https://doi.org/10.12688/f1000rese.arch.7563.2>.
77. Love MI, Huber W, Anders S. Moderated estimation of fold change and dispersion for RNA-seq data with DESeq2. *Genome Biol*. 2014;15(12):550. <https://doi.org/10.1186/s13059-014-0550-8>.
78. The Gene Ontology Consortium. The gene ontology resource: 20 years and still going strong. *Nucleic Acids Res*. 2018;47(D1):D330-D338. <https://doi.org/10.1093/nar/gky1055>.
79. Ashburner M, Ball CA, Blake JA, et al. Gene ontology: tool for the unification of biology. *Nat Genet*. 2000;25(1):25-29. <https://doi.org/10.1038/75556>.
80. Sergushichev AA. An algorithm for fast preranked gene set enrichment analysis using cumulative statistic calculation. *bioRxiv*. 2016;060012. doi:<https://doi.org/10.1101/060012>.
81. Conway JR, Lex A, Gehlenborg N. UpSetR: an R package for the visualization of intersecting sets and their properties. *Bioinformatics*. 2017;33(18):2938-2940. <https://doi.org/10.1093/bioinformatics/btx364>.
82. Wickham H. *Ggplot2: Elegant Graphics for Data Analysis*. New York: Springer-Verlag; 2016.

SUPPORTING INFORMATION

Additional supporting information may be found online in the Supporting Information section at the end of this article.

How to cite this article: Mathew AS, Gorick CM, Thim EA, et al. Transcriptomic response of brain tissue to focused ultrasound-mediated blood-brain barrier disruption depends strongly on anesthesia. *Bioeng Transl Med*. 2021;6:e10198. <https://doi.org/10.1002/btm2.10198>